PNAS RESEARCH ARTICLE | BIOPHYSICS AND COMPUTATIONAL BIOLOGY
MICROBIOLOGY

In situ NMR reveals a pH sensor motif in an outer membrane protein that drives bacterial vesicle production

Nicholas A. Wood[a], Alyssa Kraft[a], Kyungsoo Shin[a], Tata Gopinath[a], and Francesca M. Marassi[a,1]

Edited by Robert Tycko, National Institutes of Health, Bethesda, MD; received January 21, 2025; accepted May 6, 2025

The outer membrane vesicles (OMVs) produced by diderm bacteria have important roles in cell envelope homeostasis, secretion, interbacterial communication, and pathogenesis. The facultative intracellular pathogen *Salmonella enterica* Typhimurium (STm) activates OMV biogenesis inside the acidic vacuoles of host cells by upregulating the expression of the OM protein PagC, one of the most robustly activated genes in a host environment. Here, we used solid-state nuclear magnetic resonance (NMR) and electron microscopy (EM), with native bacterial OMVs, to demonstrate that three histidines, essential for the OMV biogenic function of PagC, constitute a key pH-sensing motif. The NMR spectra of PagC in OMVs show that they become protonated around pH 6, and His protonation is associated with specific perturbations of select regions of PagC. The use of bacterial OMVs is a key aspect of this work enabling NMR structural studies in the context of the physiological environment. PagC expression upregulates OMV production in *Escherichia coli*, replicating its function in STm. Moreover, the presence of PagC drives a striking aggregation of OMVs and increases bacterial cell pellicle formation at acidic pH, pointing to a potential role as an adhesin active in biofilm formation. The data provide experimental evidence for a pH-dependent mechanism of OMV biogenesis and aggregation driven by an OM protein.

outer membrane vesicle | solid-state NMR | PagC | *Salmonella*

Significance

The *Salmonella* surface protein PagC is a major driver of extracellular vesicle formation. Here, we show that this phenotype is transferrable to *Escherichia coli*, another diderm, Gram-negative bacterium. PagC increases vesicle production in *E. coli*. Three histidines, essential for vesiculation, become protonated at acidic pH, and acidic pH promotes aggregation of bacterial cells and outer membrane vesicles (OMVs). NMR of PagC in native vesicles is introduced as an important tool for in situ structural analysis of bacterial membrane proteins. The results have important implications for understanding the factors that drive the bacterial extracellular vesicle secretion, as well as their roles as vaccine, drug delivery, and nanotechnology platforms.

Extracellular vesicle secretion is a fundamental membrane remodeling process shared by eukaryotic and prokaryotic cells across all kingdoms of life. In diderm bacteria, including Gram-negative species, the vesicles released from the outer membrane (OM) perform many functions important for host infection, environmental adaptation, and colonization and also have important roles as vaccine, drug delivery, and nanotechnology platforms (1–3). While curvature-inducing proteins are known to play prominent roles in actively driving eukaryotic membrane remodeling and vesiculation by scaffolding or wedging (4, 5), the mechanisms governing prokaryotic membrane curvature and OM vesicle (OMV) biogenesis are not well understood and generally thought to be more passive processes driven by disruption of OM-peptidoglycan connections, periplasmic accumulation of misfolded biomolecules, or incorporation of modified LPS in the outer leaflet of the OM (1–4). In this study, we present evidence that the OM protein PagC, which promotes OM vesiculation in *Salmonella* (6–8), acts as a pH sensor and active driver of OMV biogenesis and can confer this phenotype to another Gram-negative bacterium, *Escherichia coli*.

In *Salmonella*, PagC expression is induced by the PhoPQ regulon upon exposure to acidic pH, divalent cation limitation, or cationic antimicrobial peptides (9–11). Notably, PagC is sufficient for promoting OMV production by *Salmonella enterica* serovar Typhimurium (STm), even in the absence of LPS-modifying enzymes (7, 8). The vesiculation activity is largely localized to two sequences harboring three histidines (H60, H62, and H102) in the second and third extracellular loops (EL2 and EL3) of its predicted eight-stranded β-barrel structure (8) (Fig. 1 and *SI Appendix*, Fig. S1). This locus is an attractive candidate for a pH-sensing motif because the typical acid dissociation constant (pKa~6) of His sidechains makes them susceptible to protonation and positive charge acquisition in the acidic intravacuolar environment encountered by STm during infection (9–11).

Given that acidic pH is one of the most potent activating signals for the PhoPQ regulon, the subset of activated genes, including PagC, may be expected to respond to environmental pH. Indeed, mimicking acidic conditions by mutating His to positively charged Lys generates a superactivated PagC mutant that overproduces OMVs compared to wild-type, while mutations to Ala dramatically suppress OMV production (8). Molecular dynamics (MD) simulations (8) suggest that PagC can alter its shape and dynamics from a cylinder at neutral pH, to a wedge at acidic pH. This could induce OM curvature and vesiculation, but whether the PagC histidines are susceptible to protonation, and whether PagC undergoes conformational change, have remained open questions.

Author affiliations: [a]Department of Biophysics, Medical College of Wisconsin, Milwaukee, WI 53226-3548

Preprint server: bioRxiv.

Author contributions: N.A.W., K.S., T.G., and F.M.M. designed research; N.A.W., A.K., and T.G. performed research; N.A.W., K.S., T.G., and F.M.M. analyzed data; and N.A.W., K.S., T.G., and F.M.M. wrote the paper.

The authors declare no competing interest.

This article is a PNAS Direct Submission.

[1]To whom correspondence may be addressed. Email: fmarassi@MCW.edu.

This article contains supporting information online at https://www.pnas.org/lookup/suppl/doi:10.1073/pnas.2501638122/-/DCSupplemental.

Published June 24, 2025.

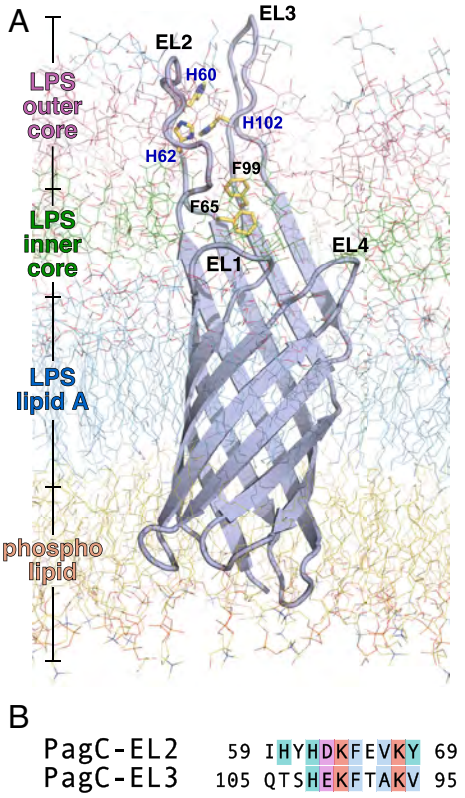

Fig. 1. Structural model of PagC. (*A*) Representative structure of PagC, taken at 2,998 ns of MD simulation (8) in the OM, showing the three His and two Phe side chains (yellow sticks) in the proposed pH-sensing motif. The OM includes LPS (blue, green, and pink lines) and phospholipid (yellow lines). (*B*) Inverse sequence alignment of the ascending and descending neighboring segments of EL2 and EL3. Alignments are rendered with ClustalX coloring.

Here, we used solid-state NMR and electron microscopy (EM), with PagC in *E. coli* bacterial OMVs, to analyze the effects of pH on His protonation, PagC conformation, and OMV structure. The data show that H60, H62, and H102 become protonated at acidic pH, and acidic pH induces specific changes in select regions of the protein. PagC expression appears to promote OMV production in *E. coli*, replicating its function in STm and reinforcing its role as a unique active driver of OMV biogenesis. Moreover, acidic pH induces extensive OMV autoaggregation and bacterial cell pellicle formation, suggesting a potential role of PagC in biofilm formation. The data point to an active mechanism for pH-dependent modulation of OMV biogenesis by a bacterial OM protein.

Results and Discussion

PagC Localizes to *E. coli* OMVs. Bacterial OMVs have the same membrane organization as the parental bacterial OM, including an inner leaflet composed of phospholipids, an outer leaflet composed of LPS, and various OM proteins (Fig. 1*A*). This highly asymmetric membrane organization is essential for supporting protein structure and function (12, 13) yet not easily mimicked in samples reconstituted from purified components. To analyze the structure and activity of PagC in the native context, we sought to work with native OMVs isolated from bacteria modified only by an inducible *pagC* gene. Since *E. coli* has been shown to support activities of PagC (14), we transformed Lemo21(DE3) *E. coli* cells with a *pagC*-encoding, IPTG-inducible plasmid and isolated OMVs from the culture media for analysis.

SDS-PAGE and western blots (Fig. 2*A*) show that the resulting OMVs are enriched in plasmid-encoded PagC (pPagC) relative to whole cells, as reported for STm (8). The appearance of a heat-modifiable band that shifts from ~14 kDa to 18 kDa upon heat denaturation demonstrates that the protein is folded and behaves as an integral membrane β-barrel. OMVs isolated from cells transformed with empty plasmid vector (pEV), but otherwise cultured and induced as pPagC cells, do not contain PagC and therefore serve as a valuable negative control. As a further control, we isolated OMVs from cells expressing plasmid-encoded Ail (pAil), the PagC homolog from the pathogen *Yersinia pestis*. Like PagC, Ail localizes to both the *E. coli* cell OM and secreted OMVs and displays the characteristic heat modifiability of OM β-barrels (Fig. 2*B*).

All three OMV types (pPagC, pEV, and pAil) are highly enriched in the major porin OmpF, as evidenced by SDS-PAGE and mass spectrometry. OmpF facilitates the general passive diffusion of polar molecules (600 to 700 Da) across the OM (15) and is a known component of the OMV proteome (16) where it supports the exchange of solutes and protects vesicle structures from osmotic stress. Interestingly, SDS-PAGE densitometry indicates that while Ail resides primarily in the cellular OM (Ail/OmpF = 26/74 in OMVs), PagC is preferentially enriched in OMVs (PagC/OmpF = 68/32 in OMVs). The localization of PagC to *E. coli* OMVs is in line with its reported behavior in STm (7) and points to a specific property that distinguishes it from its homolog Ail.

Cryogenic EM shows that both pPagC and pEV OMVs adopt discrete spherical structures (Fig. 2 *C* and *D*), with a distinct single membrane and the two leaflets of the lipid bilayer clearly resolved in electron-dense regions, as described for OMVs from other diderm bacteria (17). Moreover, negative stain EM shows that pPagC, pEV, and pAil OMVs each have relatively uniform size (Fig. 2 *E*–*G*), but PagC expression increases the average OMV diameter to 41.3 nm compared to the averages of 34.2 and 35 nm observed for pEV and pAil OMVs (Fig. 2*H*). The results are in line with size estimates of STm OMVs in the 20 to 40 nm range based on transmission EM but differ from the larger (~165 nm) diameter estimates based on nanoparticle tracking analysis (7, 18–20). As noted previously (7), these differences reflect the experimental sizing approaches: Nanoparticle tracking, commonly used in extracellular vesicle studies, fails to report vesicle diameters below 60 nm (21), while an important advantage of EM is the ability to select only biogenic OMVs and exclude the typically larger and often multilamellar vesicular structures that can result from explosive cell lysis (*SI Appendix*, Fig. S2). Thus, we conclude that biogenic OMVs of similar shape and size are observed in engineered *E. coli* as in STm.

Finally, PagC expression appears to result in approximately two-fold higher yield of OMVs compared to either pEV or pAil, as estimated by both light scattering and UV absorbance (Fig. 2*I*). The data therefore indicate that the vesiculation activity of PagC observed in STm (7, 8) is also reproduced in *E. coli*, and provide further evidence that OMV activation is a PagC-specific property.

Solid-State NMR Analysis of PagC OMVs. Solid-state NMR is ideally suited for structural studies of integral membrane proteins in lipid assemblies, including bacterial cell envelopes and membranes (22–24). Here, we took biogenic OMVs isolated from *E. coli* directly for solid-state NMR analysis. To achieve PagC-targeted ^{15}N and ^{13}C isotope labeling, and suppress NMR signals arising from endogenous *E. coli* proteins, we used a protocol where the T7/DE3-mediated expression of plasmid-encoded PagC is coupled with the suppression of chromosomal gene transcription by the antibiotic rifampicin (25, 26). The cells were first grown in unlabeled minimal media and only transferred to isotopically labeled media to induce protein expression. OMVs were isolated from the culture media and packed into 3.2 mm magic angle spinning (MAS) rotors for NMR experiments.

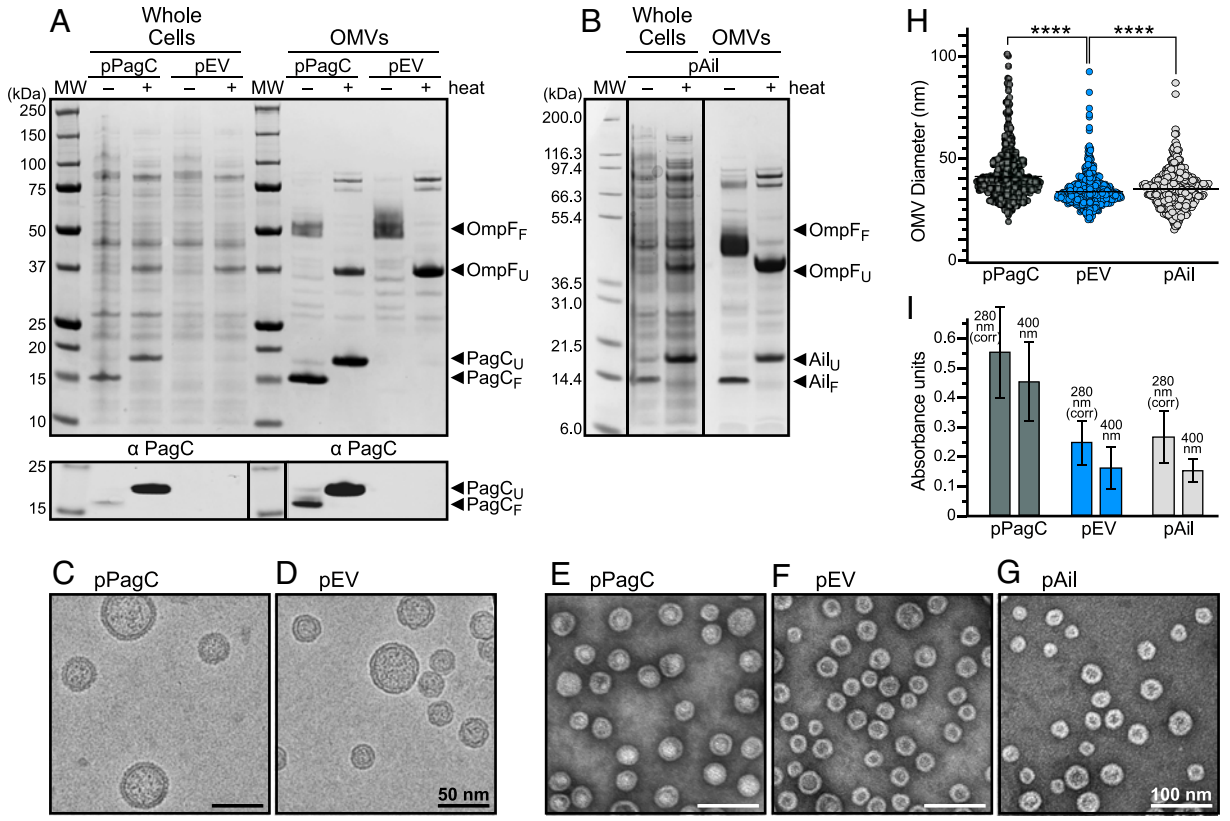

Fig. 2. PagC expressed in *E. coli* localizes to OMVs. (*A* and *B*) SDS-PAGE of whole cells and OMVs isolated from pPagC, pEV (empty plasmid), or pAil bacteria. Proteins were visualized with Coomassie stain (*Top*) or immunoblotting with PagC-specific antibody (α-PacC, *Bottom*). Arrows mark bands from folded (F) and heat-unfolded (U) proteins. (*C*–*G*) Representative cryo-EM (*C* and *D*) or negative stain EM (*E*–*G*) of pPagC, pEV, and pAil OMVs at pH 7. (*H*) OMV size estimates from negative stain EM analysis. For each of pPagC, pEV, or pAil *E. coli*, 500 OMVs were selected for analysis using FIJI. Statistical significance (n ≥ 3 biological replicates) was calculated using unpaired Student's two-tailed test and set at a *P* value < 0.05 (****$P < 0.0001$). (*I*) Measurement of light absorbance at 400 and 280 nm for pPagC, pEV, or pAil *E. coli*. A_{280} measurements were corrected for light scattering at 380 and 400 nm. Bars represent mean values and error bars SEM (seven biological replicates).

The ^{15}N and ^{13}C spectra of pPagC OMVs (Fig. 3, black), obtained with ^{1}H-^{15}N, ^{1}H-^{13}C, and ^{1}H-^{15}N-^{13}C cross-polarization (CP), contain signals from protein, as well as lipid and LPS acyl chains, glycans, aminoglycans and potentially peptidoglycan. These cellular building blocks continue to be produced and incorporate ^{13}C and ^{15}N during the isotope labeling period of cell culture and are known components of the bacterial OMV lumen (1–3). Their NMR signals have been observed in the spectra of cell envelope samples (24, 27, 28) and may be assigned by comparison.

By contrast, little evidence of protein NMR signals is seen in the spectra of pEV OMVs, isolated from cells transformed with empty plasmid vector, but otherwise grown and induced in an identical manner as pPagC cells (Fig. 3, blue). The ^{13}C spectrum obtained by ^{1}H-^{13}C CP has both greater lipid signal intensity at 33 ppm (~30%), as well as much lower protein signal at 54 ppm (~60%) and 19 ppm (100%), for pEV versus pPagC OMVs (Fig. 3*B*), and the ^{13}C spectrum obtained by ^{1}H-^{15}N-^{13}C polarization transfer shows a dramatic signal reduction (Fig. 3*C*).

The two-dimensional $^{13}C/^{13}C$ correlation spectrum of pPagC OMVs (Fig. 3*D*, black) has many resolved signals from Ala, Ile, Pro, Ser, and Thr spin systems. These can be easily identified based on their characteristic chemical shifts at positions consistent with β-strand structure. By contrast, the spectrum of pEV OMVs (Fig. 3*D*, blue) has no detectable signals from protein, confirming that the expression system leads to highly selective isotope labeling of the target with minimal background, notwithstanding the abundance of OmpF and other proteins in the OMVs.

The Histidines of PagC Are Sensitive to pH. The proposed pH sensing motif of PagC comprises two inverse homology sequences (Fig. 1 and *SI Appendix*, Fig. S1) each located in the descending segment of EL2 (residues 62 to 69) and ascending segment of EL3 (residues 95 to 102). MD simulations (8) revealed a role for these sites in forming a series of EL2-EL3 cross contacts, including H60/H62-H102 and F65-F99 ring stacking, that stabilize the loop conformations and couple their dynamics. By contrast, protonated His generate electrostatic repulsions that decouple EL2 and EL3, altering both the conformation of PagC and its interactions with OM lipids and LPS. This model aligns with the known low pH activation of PagC and the His mutagenesis data (8), but neither His protonation in the bacterial OM nor the existence of an EL2-EL3 pH sensing motif that can switch conformation upon transfer to acidic environments, has been explored experimentally.

To address the question of His protonation, we acquired ^{15}N NMR spectra for a series of pPagC OMVs incubated in buffers ranging from pH 8.5 to pH 4 (Fig. 4*A*). The ^{15}N chemical shift tensors of His imidazole Nd and Ne nitrogens are well characterized, and isotropic ^{15}N chemical shifts are good indicators of both His protonation and hydrogen bonding (29–32). Environmental pH has a dramatic effect on the ^{15}N spectra of the His imidazole nitrogens of PagC. At pH 8.5, a broad envelope of signal intensity is observed between 172 and 260 ppm. Based on reported values of His ^{15}N chemical shifts (29–32), the 172 to 182 ppm intensity may be assigned to protonated Ne and Nd, while the weak 245 to 260 ppm signal likely reflects deprotonated nitrogens which are more challenging to detect by ^{1}H-^{15}N CP due to the lack of bound hydrogen. Overall, the absence of resolved peaks, combined

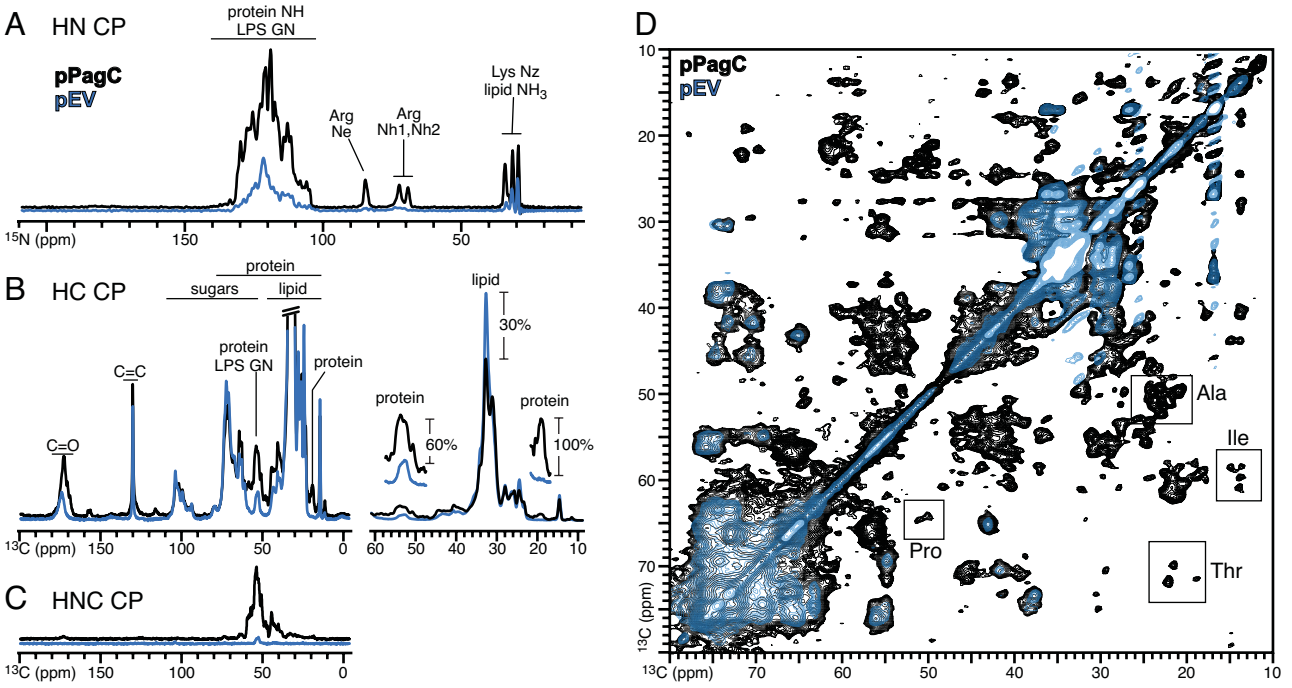

Fig. 3. NMR spectra of PagC in *E. coli* OMVs. Spectra were acquired at 4 °C for pPagC (black) or pEV (blue) OMVs at pH 7. (*A*–*C*) One-dimensional spectra acquired with ^{1}H-^{15}N CP (*A*), ^{1}H-^{13}C CP (*B*), or ^{1}H-^{15}N followed by ^{15}N-^{13}C CP (*C*). Signals from protein and LPS sites are marked (LPS GN: glucosamine). (*D*) Two-dimensional ^{13}C/^{13}C correlation PDSD spectra. Assignments to residue types are marked in *Inset* boxes.

with the weak broad signal intensity near 207 ppm, reflect a mix of neutral tautomeric states with either Nd (τ tautomer) or Ne (π tautomer) protonation, exchanging slower than the μs timescale of the ^{15}N NMR experiment (Fig. 4*B*).

As the pH is lowered, the 207 ppm intensity disappears, and resolved spectral components between ~172 and 181 ppm grow in intensity with progressive line narrowing. Three signals resolved at pH 6, and four resolved at pH 5 and pH 4, may be assigned to protonated Ne and Nd of the imidazolium cation. The signal observed at 180.1 (pH 4) and 181.1 ppm (pH 6 and pH 5) is consistent with hydrogen bonding of a protonated imidazole nitrogen to a carboxylate group (32).

The spectra are complex. The observation of three to four ^{15}N signals for three His may reflect rapid imidazole ring rotations that average the two chemically inequivalent Ne and Nd sites of each His, spectral overlap of distinct Ne and Nd signals, or selective detection of specific His residues with favorable hydrogen bonding or dynamics for NMR observation by CP. Absent resonance assignment, it is impossible to distinguish among these mechanisms, but the data unequivocally demonstrate that the His of PagC are water-accessible and sensitive to environmental pH and protonation near pH 6.

Effect of pH on the Conformation of PagC. To probe the effect of pH on other protein sites, we acquired ^{15}N/^{13}C and ^{13}C/^{13}C correlation spectra of pPagC OMVs exposed to either pH 7 or pH 4 buffer (Fig. 5 *A* and *B* and *SI Appendix*, Figs. S3 and S4). Both ^{15}N/^{13}C and ^{13}C/^{13}C spectra compare favorably with those of the PagC homolog Ail in the bacterial cell envelope (24, 33), demonstrating the potential of NMR characterization of membrane proteins in biogenic OMVs. The NMR signal intensity is ~50% greater at pH 4 than pH 7, and the number of scans was adjusted to compensate for this difference (*SI Appendix*, Table S1), which likely arises from a strong OMV aggregation effect observed at pH 4 (see below) allowing us to pack more sample into the rotor, and potentially some enhancement of ^{1}H-^{13}C CP due to increased protonation of exchangeable sites.

The ^{15}N/^{13}C spectra acquired with transfer echo double resonance (TEDOR) mixing have excellent signal intensity and resolution, with line widths of well-resolved signals in the range of 0.6 to 0.8 ppm for ^{13}C, and 1.3 to 1.8 ppm for ^{15}N (*SI Appendix*, Fig. S3). Many signals can be resolved from the eighteen Gly, four Pro, six Thr, nine Ala, and seven Ile in the sequence, including Pro N-Ca and N-Cd correlations. Since these residues are distributed across the length of the PagC β-barrel their NMR signals are valuable probes of protein conformation (Fig. 5 *C* and *D*).

The ^{15}N and ^{13}C chemical shifts from these sites reflect β-stranded secondary structure, and the spectra obtained at pH 7 and pH 4 display extensive signal overlap, indicating that the

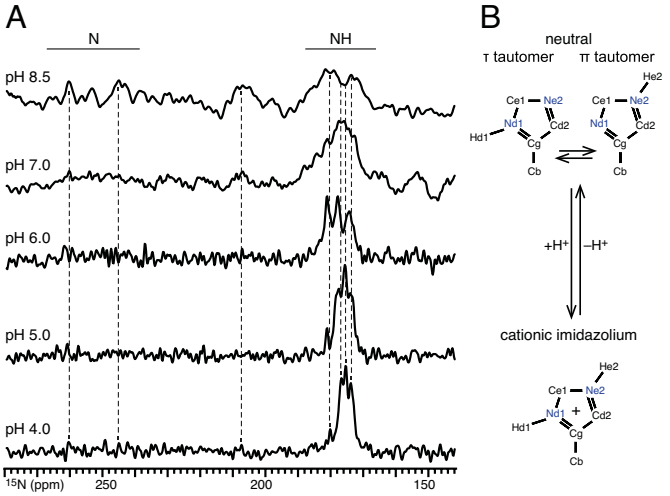

Fig. 4. pH titration of PagC His. (*A*) One-dimensional ^{15}N spectra of pPagC OMVs acquired at 4 °C with ^{1}H-^{15}N CP at pH 4 (8,000 scans), pH 5 (30,000 scans), pH 6 (86,000 scans); pH 7 (117,000 scans); and pH 8 (160,000 scans). The spectra were processed with a shifted sine bell function (SSB = 3) for pH 4 to 6, or exponential line broadening functions for pH 7 (LB = 50) and pH 8.5 (LB = 100). Dashed lines align with resolved signals. (*B*) Structures of the tautomeric states of the neutral His imidazole ring and fully protonated imidazolium cation.

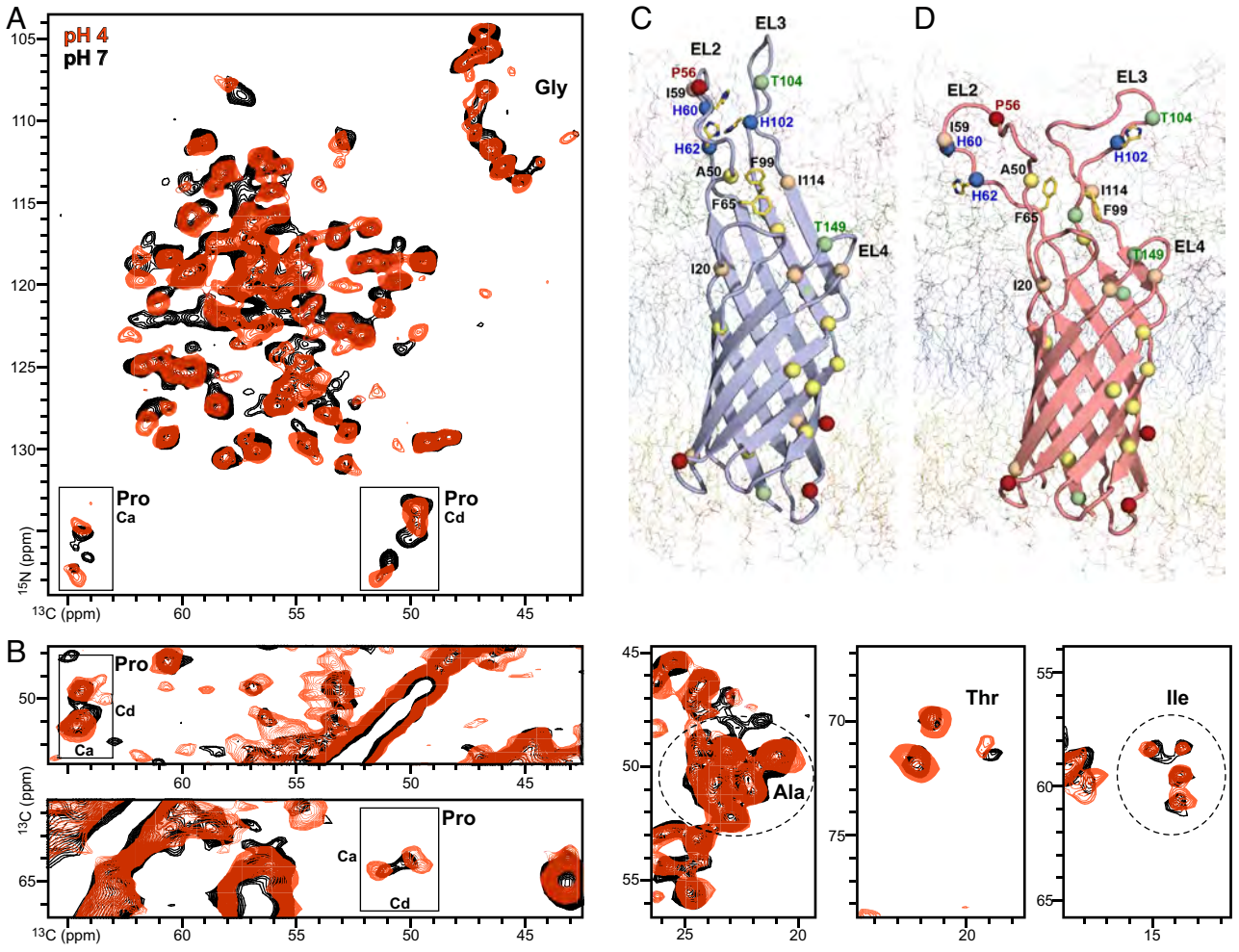

Fig. 5. Effect of pH on the $^{15}N/^{13}C$ and $^{13}C/^{13}C$ NMR spectra of PagC in *E. coli* OMVs. Spectra were acquired at 4 °C for pPagC OMVs at pH 7 (black) or pH 4 (red). (*A*) Two-dimensional $^{15}N/^{13}C$ TEDOR NCA spectra. (*B*) Two-dimensional $^{13}C/^{13}C$ PDSD spectral regions selected to show signals from Pro, Ala, Thr, and Ile. (*C* and *D*) Structural models taken from MD simulations (8) of His-neutral (*C*; 2,998 ns) or His-protonated (*D*; 2,668 ns) PagC, showing His and Phe sidechains (yellow stick), and CA atoms (sphere) of Ala (yellow), Ile (wheat), Pro (red), and Thr (green). The OM includes LPS (blue, green, and pink lines) and phospholipid (PL: yellow lines).

overall conformation of PagC is maintained irrespective of pH. Notably, there are also several ^{15}N and ^{13}C chemical shift perturbations of select signals. For example, two Thr (T98 and T104) are located in EL3 and two Thr signals are perturbed by pH in the $^{13}C/^{13}C$ spectrum (Fig. 5*B* and *SI Appendix*, Fig. S4). Moreover, select signals from hydrophobic Ala and Ile, and at least two of the Pro Ca-Cd signals, are perturbed in response to pH. While the lack of resonance assignments precludes a detailed spectral analysis, such selective peak perturbation reflects a site-specific response to the local environment of neighboring protein and LPS moieties, rather than a wholesale effect of buffer pH. Structure determination will be needed to determine the specific conformational change elicited by pH.

PagC Induces OMV Autoaggregation and Pellicle Formation at Acidic pH. In the process of NMR sample preparation, we noticed a marked flocculation of pPagC OMVs occurring immediately upon transfer to pH 4, and this prompted us to examine the ultrastructural impact of pH. Negative stain EM of freshly prepared OMVs reveals striking aggregation of pPagC but not pEV OMVs at acidic pH (Fig. 6*A* and *SI Appendix*, Fig. S5). While all OMVs are well dispersed at pH 7.5, pPagC OMVs lightly cluster at pH 6, and the dominant features at pH 5 and pH 4 are extensive aggregates with clear evidence of membrane fusion and some structures resembling wire-like OMV connections (Fig. 6*A*, arrow) similar to those described for *Myxococcus xanthus* (34). Although we could identify some solitary nonaggregated vesicles, their abundance was substantially reduced relative to neutral pH. Aggregation appears to initiate around pH 6 and complete fusion is observed at pH 4.

To test the reversibility of this phenomenon, we performed EM on pPagC OMVs incubated first at pH 4 overnight and then switched to pH 7.5 for another 12 h (Fig. 6*B* and *SI Appendix*, Fig. S5). Although many aggregate masses remain, some are visibly dissolved, suggesting some degree of reversibility. Tightly associated OMVs appear to form a mosaic-like structure in which the vesicle membranes flatten against each other increasing the contact surface. Moreover, some membranes appear to have fused, suggesting not only that PagC promotes aggregation but also that it may mediate membrane fusion.

Finally, we tested the ability of PagC to induce *E. coli* cell pellicle formation at pH 7.6 and pH 5.8 where its OMV-producing activity in STm is documented (8). At pH 7.6 there is minimal evidence of pellicle formation at the air–water interface, but a substantial pellicle forms at pH 5.8 as readily visualized by staining with crystal violet (Fig. 6*C* and *SI Appendix*, Fig. S6). By contrast, pEV cells form very little pellicle at either neutral or acidic pH, while pAil cells produce dense pellicles regardless of pH, in line with the documented aggregation activity of Ail in both its native *Y. pestis* and *E. coli* (24, 35).

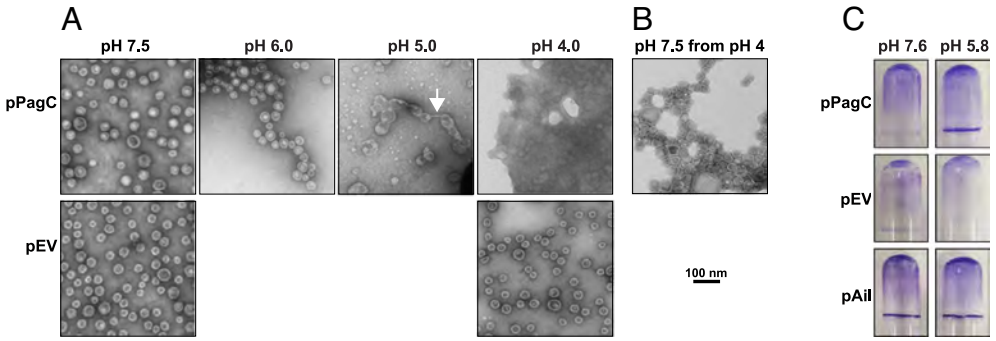

Fig. 6. PagC induces pH-dependent OMV aggregation and bacterial cell pellicle formation. (*A* and *B*) Representative negative stain EM of pPagC (*Top*) and pEV (*Bottom*) OMVs, acquired at pH 7.5, pH 6, pH 5, pH 4 (*A*) or pH 7.5 after incubation at pH 4 (*B*). The white arrow points to a wire-like OMV connection at pH5. (*C*) Pellicle formation by pPagC, pEV, and pAil *E. coli* cells. Cells were suspended in 2 mL of M9 minimal media (OD_{600} = 0.5) in 15 × 100 mm glass tubes and incubated for 16 h at 37 °C. After removing the cells by centrifugation, the interior glass walls were treated with methanol and air dried overnight, then washed three times with buffer, treated with 2.5 mL of crystal violet solution (0.1% for 10 min), then washed with buffer, and air dried. Pellicle formation was detected as a violet-stained rim at the air–water interface.

These results align with the reported association of PagC with biofilm formation and multiple drug resistance in *S. enterica* (36) as well as growing evidence that OMVs are common constituents of the microbial biofilm extracellular matrix and play an active role in biofilm formation (37–41). The pH-dependent reversible aggregation may reflect a mechanism for environmental adaptation whereby secreted OMVs aggregate to form an adhesive matrix at low pH, that can be quickly undone upon transfer to a neutral pH environment. Such a process could be important for the survival of *Salmonella* in environments of extreme pH fluctuation, such as the human digestive tract. The aggregation phenotypes remain to be demonstrated in *Salmonella*. Nontyphoidal *Salmonella* produce an alternative group IV O-antigen capsule that is implicated in environmental survival, immune evasion, and biofilm formation (42–45), while the LPS core of *E. coli* B strains, including Lemo21(DE3) used in this study, lacks O-antigen repeats and capsular biosynthesis (46, 47) and thus may artificially unmask PagC exposing its loops to the OMV surface and activating aggregation.

Conclusions

OMV secretion is a major membrane remodeling process essential for bacterial colony behavior and environmental adaptation. Recently (8), we proposed that His protonation drives a conformational change of PagC from an ordered cylindrical barrel to a wedge, where EL2 and EL3 are decoupled and exert pressure on the outer leaflet of the OM, resulting in curvature and vesicle budding. Here, we have shown that the histidines of PagC are indeed pH-sensitive and their protonation is associated with perturbations of specific PagC sites. The NMR spectra show that PagC adopts an overall β-stranded conformation in bacterial OMVs and the His sidechains titrate from neutral tautomeric states to the protonated imidazolium cation near pH 6. Whether Asp and Glu residues in the extracellular loops are also susceptible to protonation and contribute to conformational change is an interesting question that should be addressed in future studies. Overall, the NMR data reflect a specific response of PagC to environmental pH and provide experimental support for an active role as a pH sensor and driver of OM curvature.

The use of bacterial OMVs is an essential aspect of our study enabling structural analysis in the context of the native environment. Working with native samples is particularly important for bacterial OM proteins, which have coevolved with LPS to confer species-specific properties and function as a coordinated assembly with the highly asymmetric environment of the OM (12, 13). Here, the OMV-producing activity of PagC observed in STm was recapitulated in a B strain *E. coli* derivative, and the propensity of PagC to promote OMV aggregation and bacterial pellicle formation at low pH was identified as a potentially important property of this protein. With the caveat that the R1 type LPS of our B strain *E. coli* may unmask the PagC aggregation phenotype, this finding aligns with evidence for the association of PagC with biofilm formation and multiple drug resistance in *S. enterica* (36).

OMVs isolated from engineered *E. coli* have been proposed as an in situ platform for solution NMR studies of periplasmic proteins or periplasmic domains of membrane proteins (48). This application, however, relied on the deletion of multiple OM protein genes and vesicle size homogenization by filtered extrusion. Moreover, the use of solution NMR excludes the possibility of examining integral membrane proteins whose dynamics are coupled to the relatively immobile OMV structure. Here, we took native *E. coli* OMVs with the full complement of endogenous, chromosomally encoded OM proteins, directly for solid-state NMR analysis. This work, therefore, paves the way for NMR studies of physiological bacterial OMVs, including those produced by *Salmonella* and other pathogens.

In conclusion, this study provides experimental evidence for the role of PagC as an active pH sensor and a driver of OMV biogenesis, it describes a potential role of PagC as a regulator of OMV aggregation and pellicle formation, and introduces OMVs as an important platform for in situ NMR structural analysis of OM proteins.

Materials and Methods

Bacterial Strains, Culture Conditions, and Key Reagents. All *E. coli* were commercially available Lemo21(DE3) (New England BioLabs, MA). The pET22b(+)-*pagC* plasmid (pPagC) for IPTG-inducible expression of PagC lacking the endogenous signal peptide was designed in-frame with the PelB signal peptide (49) and acquired from Genscript (Piscataway, NJ). The Empty vector bacteria were transformed with empty pET22b(+) plasmid (pEV). The plasmid for IPTG-inducible expression of Ail (pAil) was described previously (24). Western blots were performed with a custom (Thermo Fisher Scientific, IL) polyclonal antibody against the PagC EL3 peptide CDGDSFSNKISSRKTGFAWG. Bacteria were cultured in M9 media supplemented with 0.2% glucose, 100 μg/mL ampicillin, and 35 μg/mL chloramphenicol when appropriate. SDS-PAGE band densitometry was analyzed using VisionWorks 4+ (Analytik Jena), Fiji Image J, and Adobe Photoshop, and the average value taken.

Isotope Labeling of PagC. Transformed bacteria (pPagC, pEV, and pAil) were grown overnight at 37 °C in unlabeled M9 media. Overnight cultures were used to inoculate fresh unlabeled M9 to achieve OD_{600} = 0.1 and cells were incubated with shaking at 37 °C. At OD_{600} = 0.6, expression of the DE3 RNA polymerase was

induced by adding 0.4 mM IPTG. Following a 10-min incubation, the cells were pelleted (5,000 × g, 4 °C, 20 min) and resuspended in M9 supplemented with 1 g/L of ^{15}N ammonium sulfate and 0.2% ^{13}C glucose (Cambridge Isotope Laboratories, MA), IPTG and rifampicin were added to 0.4 mM and 100 μg/mL, respectively, and expression was allowed to proceed for 16 h at 26 °C prior to harvesting.

OMV Isolation and Characterization. OMVs were harvested by diafiltration and ultracentrifugation. The cultures were centrifuged (5,000 × g, 4 °C, 20 min) to remove bacterial cells, and the resulting supernatants were centrifuged again to remove residual bacteria. This supernatant was passed through a 0.45 μm filter to remove residual bacteria and large aggregates, and the filtrate was concentrated using an Amicon stirred cell fitted with a 300 kDa PES membrane disc filter (Millipore Sigma, St. Louis, MO). OMVs in the concentrated filtrates were harvested by centrifugation (150,000 × g, 4 °C, 1.5 h), and resuspended in buffer for analysis. All OMV buffers contained 0.9 mM $CaCl_2$ and 0.5 mM $MgCl_2$ to preserve OMV membrane integrity as previously described (50). OMVs were quantified by light scattering and UV absorbance, as described (50, 51).

Cryo-EM. Purified OMVs (3 μL of ~1 mg/mL) were applied to a glow-discharged Quantifoil 300-mesh gold grid in a Vitrobot chamber (ThermoFisher Mark IV). Excess liquid was blotted with a blot force of 3, blot time of 6 s, and the grid was plunge-frozen into liquid ethane. Imaging was performed on a ThermoFisher Glacios 200 kV electron microscope equipped with a Falcon 4 direct electron detector, and Selectris energy filter. Micrographs were collected with a magnification of 100 kx, a pixel size of 1.089 Å/pixel, and a total dose of 60 $e^-/Å^2$. Images were processed using Cryosparc v4.4.

Negative Stain EM. Samples were adsorbed onto glow-discharged 400 mesh Formvar carbon copper grids (Electron Microscopy Sciences, PA) for 15 s, and then wicked away with filter paper. The grids were then treated with 2% uranyl-acetate for 30 s, then blotted to remove the stain, and allowed to dry for at least 1 h prior imaging at 100,000× magnification on a Jeol JEM-1400 Transmission Electron Microscope (JEOL USA, MA) at 60 kV. For each experiment, 500 OMVs were selected for measurement using FIJI (52).

Solid-State NMR Spectroscopy. OMV samples were centrifuged into 3.2 mm zirconium rotors for solid-state NMR. Solid-state NMR experiments were performed on a 700 MHz AVANCE NEO Bruker spectrometer, equipped with a 3.2 mm E-free $^1H/^{13}C/^{15}N$ probe. All experiments were acquired at a sample temperature of 4 °C, with a MAS rate of 12.5 kHz, and a recycle delay of 2 s. The 90° pulse lengths for ^1H, ^{13}C, and ^{15}N were set to 3 μs, 6 μs, and 6 μs. Heteronuclear decoupling was achieved using the spinal-64 pulse sequence with 70 kHz radiofrequency amplitude. During ^1H-^{13}C and ^1H-^{15}N CP, 30 kHz radiofrequency amplitude was used on ^{13}C or ^{15}N channels. The Hartmann–Hahn matching condition was set by ramping the ^1H radiofrequency amplitude to maximize signal intensity. During double ^1H-^{15}N-^{13}C CP, NCA polarization transfer was obtained with 22 kHz and 32 kHz radiofrequency spinlocks on the ^{13}C and ^{15}N channels, with 70 kHz continuous-wave decoupling on the ^1H channel. For the TEDOR experiments, Hadamard encoding (53) was applied with 2 ms selective I-BURP pulses on the ^{15}N channel. NMR experimental details are provided in *SI Appendix*, Table S1.

Pellicle Formation. Pellicle formation was assayed as described (24) with minor modifications. Cells from an overnight induction were harvested by centrifugation, washed with sterile ice-cold phosphate buffer saline (PBS), and resuspended in 2 mL of M9 minimal media to OD_{600} = 0.5 in 15 × 100 mm glass tubes and incubated at 37 °C with gentle agitation for 16 h.

After removing the cell suspensions by aspiration, the interior glass walls were treated with 2.5 mL of 100% ice-cold methanol for 5 min, air-dried overnight, and then washed three times with PBS prior to staining with 0.1% crystal violet for 10 min. The tubes were treated with 2.5 mL of crystal violet solution (0.1%) for 10 min, then rinsed twice with PBS to remove excess dye, and air dried overnight prior to imaging. Pellicle formation was determined qualitatively as a violet-stained ring at the air–liquid interface.

Data, Materials, and Software Availability. Previously published data were used in this work. Figs. 1*A* and 5 *C* and *D*, from this paper (Tracking #: 2025-01638RR), are original and were not reproduced from a published article. Structural models in these figures were generated from MD simulations described in ref. 8, but the data were reanalyzed for this study. Ref. 8 is cited in the figure legends. All other data are included in the manuscript and/or *SI Appendix*.

ACKNOWLEDGMENTS. This work was supported by grants from the NIH (GM118186 and F32AI188770). It utilized NMR instrumentation supported by a grant from the NIH (OD028716), transmission EM instrumentation supported by the Medical College of Wisconsin – Oxford Instruments Center for Advanced Microscopy and EM Core, and cryo-EM instrumentation supported by the Medical College of Wisconsin Cancer Center. We thank Ashish Gadicherla and Linda Olson for their assistance with EM, and Matthew Waldor, Dieter Schifferli and Marassi lab members for discussion.

1. C. Schwechheimer, M. J. Kuehn, Outer-membrane vesicles from Gram-negative bacteria: Biogenesis and functions. *Nat. Rev.* **13**, 605–619 (2015).
2. M. G. Sartorio, E. J. Pardue, M. F. Feldman, M. F. Haurat, Bacterial outer membrane vesicles: From discovery to applications. *Annu. Rev. Microbiol.* **75**, 609–630 (2021).
3. M. Toyofuku, S. Schild, M. Kaparakis-Liaskos, L. Eberl, Composition and functions of bacterial membrane vesicles. *Nat. Rev.* **21**, 415–430 (2023).
4. O. Bohuszewicz, J. Liu, H. H. Low, Membrane remodelling in bacteria. *J. Struct. Biol.* **196**, 3–14 (2016).
5. H. T. McMahon, J. L. Gallop, Membrane curvature and mechanisms of dynamic cell membrane remodelling. *Nature* **438**, 590–596 (2005).
6. R. Kitagawa *et al.*, Biogenesis of Salmonella enterica serovar typhimurium membrane vesicles provoked by induction of PagC. *J. Bacteriol.* **192**, 5645–5656 (2010).
7. R. Dehinwal *et al.*, Increased production of outer membrane vesicles by Salmonella interferes with complement-mediated innate immune attack. *mBio* **12**, e0086921 (2021).
8. R. Dehinwal *et al.*, A pH-sensitive motif in an outer membrane protein activates bacterial membrane vesicle production. *Nat. Commun.* **15**, 6958 (2024).
9. S. I. Miller, A. M. Kukral, J. J. Mekalanos, A two-component regulatory system (phoP phoQ) controls Salmonella typhimurium virulence. *Proc. Natl. Acad. Sci. U.S.A.* **86**, 5054–5058 (1989).
10. E. A. Groisman, E. Chiao, C. J. Lipps, F. Heffron, Salmonella typhimurium phoP virulence gene is a transcriptional regulator. *Proc. Natl. Acad. Sci. U.S.A.* **86**, 7077–7081 (1989).
11. C. M. Alpuche Aranda, J. A. Swanson, W. P. Loomis, S. I. Miller, Salmonella typhimurium activates virulence gene transcription within acidified macrophage phagosomes. *Proc. Natl. Acad. Sci. U.S.A.* **89**, 10079–10083 (1992).
12. J. C. Henderson *et al.*, The power of asymmetry: Architecture and assembly of the Gram-Negative outer membrane lipid bilayer. *Annu. Rev. Microbiol.* **70**, 255–278 (2016).
13. J. E. Horne, D. J. Brockwell, S. E. Radford, Role of the lipid bilayer in outer membrane protein folding in Gram-negative bacteria. *J. Biol. Chem.* **295**, 10340–10367 (2020).
14. M. Nishio, N. Okada, T. Miki, T. Haneda, H. Danbara, Identification of the outer-membrane protein PagC required for the serum resistance phenotype in Salmonella enterica serovar Choleraesuis. *Microbiology (Reading)* **151**, 863–873 (2005).
15. S. W. Cowan *et al.*, The structure of OmpF porin in a tetragonal crystal form. *Structure* **3**, 1041–1050 (1995).
16. E. Y. Lee *et al.*, Global proteomic profiling of native outer membrane vesicles derived from Escherichia coli. *Proteomics* **7**, 3143–3153 (2007).
17. M. Kaplan *et al.*, In situ imaging of bacterial outer membrane projections and associated protein complexes using electron cryo-tomography. *Elife* **10**, e73099 (2021).
18. B. L. Deatherage *et al.*, Biogenesis of bacterial membrane vesicles. *Mol. Microbiol.* **72**, 1395–1407 (2009).
19. J. Nevermann *et al.*, Identification of genes involved in biogenesis of outer membrane vesicles (OMVs) in Salmonella enterica serovar Typhi. *Front. Microbiol.* **10**, 104 (2019).
20. P. Marchant *et al.*, "One for All": Functional transfer of OMV-mediated polymyxin B resistance from Salmonella enterica sv. Typhi DeltatolR and DeltadegS to susceptible bacteria. *Front. Microbiol.* **12**, 672467 (2021).
21. D. Bachurski *et al.*, Extracellular vesicle measurements with nanoparticle tracking analysis–An accuracy and repeatability comparison between NanoSight NS300 and ZetaView. *J. Extracell. Vesicles* **8**, 1596016 (2019).
22. L. Mao *et al.*, Suppression of phospholipid biosynthesis by cerulenin in the condensed Single-Protein-Production (cSPP) system. *J. Biomol. NMR* **49**, 131–137 (2011).
23. M. Renault *et al.*, Cellular solid-state nuclear magnetic resonance spectroscopy. *Proc. Natl. Acad. Sci. U.S.A.* **109**, 4863–4868 (2012).
24. J. E. Kent *et al.*, Correlating the structure and activity of Y. pestis Ail in a bacterial cell envelope. *Biophys. J.* **120**, 453–462 (2021).
25. F. C. Almeida *et al.*, Selectively labeling the heterologous protein in Escherichia coli for NMR studies: A strategy to speed up NMR spectroscopy. *J. Magn. Reson.* **148**, 142–146 (2001).
26. C. Cruzeiro-Silva, F. P. Albernaz, A. P. Valente, F. C. Almeida, In-Cell NMR spectroscopy: Inhibition of autologous protein expression reduces Escherichia coli lysis. *Cell Biochem. Biophys.* **44**, 497–502 (2006).
27. C. Laguri *et al.*, Solid state NMR studies of intact lipopolysaccharide endotoxin. *ACS Chem. Biol.* **13**, 2106–2113 (2018).
28. J. E. Kent, B. E. Ackermann, G. T. Debelouchina, F. M. Marassi, Dynamic nuclear polarization illuminates key protein–lipid interactions in the native bacterial cell envelope. *Biochemistry* **62**, 2252–2256 (2023).
29. G. Harbison, J. Herzfeld, R. G. Griffin, Nitrogen-15 chemical shift tensors in L-histidine hydrochloride monohydrate. *J. Am. Chem. Soc.* **103**, 4752–4754 (2002).
30. J. E. Roberts, G. S. Harbison, M. G. Munowitz, J. Herzfeld, R. G. Griffin, Measurement of heteronuclear bond distances in polycrystalline solids by solid-state NMR techniques. *J. Am. Chem. Soc.* **109**, 4163–4169 (2002).
31. A. Ramamoorthy, C. H. Wu, S. J. Opella, Magnitudes and orientations of the principal elements of the 1H chemical shift, 1H–15N dipolar coupling, and 15N chemical shift interaction tensors in

15Nε1-tryptophan and 15Nπ-histidine side chains determined by three-dimensional solid-state NMR spectroscopy of polycrystalline samples. *J. Am. Chem. Soc.* **119**, 10479–10486 (1997).
32. Y. Wei, A. C. de Dios, A. E. McDermott, Solid-state 15N NMR chemical shift anisotropy of histidines: Experimental and theoretical studies of hydrogen bonding. *J. Am. Chem. Soc.* **121**, 10389–10394 (1999).
33. S. K. Dutta, Y. Yao, F. M. Marassi, Structural insights into the Yersinia pestis outer membrane protein ail in lipid bilayers. *J. Phys. Chem. B* **121**, 7561–7570 (2017).
34. J. P. Remis *et al.*, Bacterial social networks: Structure and composition of yxococcus xanthus outer membrane vesicle chains. *Environ. Microbiol.* **16**, 598–610 (2014).
35. A. M. Kolodziejek *et al.*, Phenotypic characterization of OmpX, an Ail homologue of Yersinia pestis KIM. *Microbiology (Reading)* **153**, 2941–2951 (2007).
36. S. O. Hasson *et al.*, Intimin (eae) and virulence membrane protein pagC genes are associated with biofilm formation and multidrug resistance in Escherichia coli and Salmonella enterica isolates from calves with diarrhea. *BMC Res. Notes* **15**, 321 (2022).
37. S. R. Schooling, T. J. Beveridge, Membrane vesicles: An overlooked component of the matrices of biofilms. *J. Bacteriol.* **188**, 5945–5957 (2006).
38. N. Chen *et al.*, Bacterial extracellular vesicle: A non-negligible component in biofilm life cycle and challenges in biofilm treatments. *Biofilm* **8**, 100216 (2024).
39. A. Kulp, M. J. Kuehn, Biological functions and biogenesis of secreted bacterial outer membrane vesicles. *Annu. Rev. Microbiol.* **64**, 163–184 (2010).
40. H. C. Flemming *et al.*, Biofilms: An emergent form of bacterial life. *Nat. Rev. Microbiol.* **14**, 563–575 (2016).
41. G. O'Toole, H. B. Kaplan, R. Kolter, Biofilm formation as microbial development. *Annu. Rev. Microbiol.* **54**, 49–79 (2000).
42. D. E. Heinrichs, J. A. Yethon, C. Whitfield, Molecular basis for structural diversity in the core regions of the lipopolysaccharides of Escherichia coli and Salmonella enterica. *Mol. Microbiol.* **30**, 221–232 (1998).
43. D. L. Gibson *et al.*, Salmonella produces an O-antigen capsule regulated by AgfD and important for environmental persistence. *J. Bacteriol.* **188**, 7722–7730 (2006).
44. R. W. Crawford, D. L. Gibson, W. W. Kay, J. S. Gunn, Identification of a bile-induced exopolysaccharide required for Salmonella biofilm formation on gallstone surfaces. *Infect. Immun.* **76**, 5341–5349 (2008).
45. R. K. Ernst, T. Guina, S. I. Miller, Salmonella typhimurium outer membrane remodeling: Role in resistance to host innate immunity. *Microbes Infect.* **3**, 1327–1334 (2001).
46. E. N. Andreishcheva, W. F. Vann, Escherichia coli BL21(DE3) chromosome contains a group II capsular gene cluster. *Gene* **384**, 113–119 (2006).
47. H. Jeong *et al.*, Genome sequences of Escherichia coli B strains REL606 and BL21(DE3). *J. Mol. Biol.* **394**, 644–652 (2009).
48. J. Thoma, B. M. Burmann, High-resolution in situ NMR spectroscopy of bacterial envelope proteins in outer membrane vesicles. *Biochemistry* **59**, 1656–1660 (2020).
49. S. P. Lei, H. C. Lin, S. S. Wang, J. Callaway, G. Wilcox, Characterization of the Erwinia carotovora pelB gene and its product pectate lyase. *J. Bacteriol.* **169**, 4379–4383 (1987).
50. F. Castegnaro, B. M. Burmann, J. Thoma, Preparation of protein-enriched outer membrane vesicles from Escherichia Coli for in situ structural biology of outer membrane proteins. *Methods Mol. Biol.* **2652**, 247–257 (2023).
51. J. Thoma *et al.*, Protein-enriched outer membrane vesicles as a native platform for outer membrane protein studies. *Commun. Biol.* **1**, 23 (2018).
52. J. Schindelin *et al.*, Fiji: An open-source platform for biological-image analysis. *Nat. Methods* **9**, 676–682 (2012).
53. T. Gopinath, A. Kraft, K. Shin, N. A. Wood, F. M. Marassi, Solid state NMR spectral editing of histidine, arginine and lysine using Hadamard encoding. *J. Biomol. NMR* **79**, 35–45 (2025).